Fuel Communications 9 (2021) 100038

Contents lists available at ScienceDirect

Fuel Communications

journal homepage: www.sciencedirect.com/journal/fuel-communications

Total oxidation of carbon monoxide, VOC and reduction of NO_2 with catalytic ceramic filter media

Grazyna Straczewski [a,*], Camila Vargas [b], Ariana Zampieri [b], Krassimir Garbev [a], Hans Leibold [a], Nicolaus Dahmen [b]

[a] Institute for Technical Chemistry, Karlsruhe Institute of Technology, Hermann-von-Helmholtz-Platz 1, Eggenstein-Leopoldshafen 76344, Germany
[b] Institute for Catalysis Research and Technology, Karlsruhe Institute of Technology, Hermann-von-Helmholtz-Platz 1, Eggenstein-Leopoldshafen 76344, Germany

ARTICLE INFO

Keywords:
CO oxidation
VOC oxidation
NO_2 reduction
Copper-manganese oxide catalyst
Catalytic filter material

ABSTRACT

This paper deals with the effect of catalyst loading on the activity and selectivity of CuO_x–MnO_y catalysts on alumina-silicate supports (fiber material-Al_2O_3(44)/SiO_2(56)). A special focus lies on the oxidation of CO, on mixtures of VOC from 1-butene, isobutane, n-butane, propane, ethene, and ethane, as well as on CO oxidation in the presence of NO_2. The catalysts are prepared through wet impregnation of the filter section with an aqueous solution of copper and manganese nitrate. The rate of CO oxidation for small carbon monoxide concentrations of up to 1 vol.% is independent of catalyst loading in the filter material. In contrast, at a carbon monoxide concentration of around 3 vol.%, it is found that the rate of CO oxidation increased rapidly with increasing catalyst loading of the filter material. The highest catalytic activity of over 93% CO elimination is achieved at 290 °C for 1 vol.% CO and smaller catalyst loading and for 3 vol.% CO with higher catalyst loading. In long-term stability tests, complete CO conversion is measured without deactivating the catalyst at 390 °C for at least 100 h. The highest catalytic activity for VOC elimination of 90% is achieved in the temperature range of 350–420 °C. During the CO—NO_2 reaction with and without O_2, a constant decrease in the CO oxidation rate is observed, while the NO_2 reduction rate remained constant at a temperature below 300 °C.

Introduction

Catalytic total oxidation is widely used in several industrial processes for air pollution abatement and in particular for controlling volatile organic compounds (VOC) and carbon monoxide emissions. Thermal oxidizers or thermal incinerators are combustion systems that control VOC and CO total oxidation emissions by complete combustion to produce carbon dioxide (CO_2) and water. The design of a combustion system depends on the concentration of pollutants in the exhaust gas flow, the type of pollutant, presence of other gasses, oxygen content, and the stability of the emission. Thermal combustion takes place at temperatures above 800 °C. However, harmful by-products, such as carbon monoxide and nitrogen oxides, also occur at these temperatures and care must be taken to achieve high combustion efficiency under variable input conditions [1]. Catalytic post-combustion lowers both oxidation temperatures and fuel consumption of the combustion process [2]. The reaction temperatures can thus be reduced from 300 to 500 °C, which can lead to considerable energy and cost savings. Consequently, it is highly important to develop suitable catalysts for the efficient oxidation of CO and VOC that are present in low concentrations and for NO_x elimination in the exhaust gasses emanating from various combustion processes. Transition metal oxides, such as CuO_x [3–6], MnO_x [5–9], CeO_x [4,10–12], NiO_x [3,11], and their binary mixtures [4–6,10,12–13] are a promising choice due to their low cost, easy reducibility, high resistance to poisoning and the relatively low operating temperature.

Manganese oxides are attractive catalysts due to the labile oxygen necessary to complete a catalytic cycle. Figueroa et al. [7]. found that the catalytic activity of MnO_x catalyst is related to the presence of Mn^{3+}-Mn^{4+} couple and Mn^{4+} vacancies. Trawczyński et al. [8] studied the interaction of MnO_x with various support materials (YSZ, Al_2O_3, TiO_2) and found that reduction of MnO_x catalyst is controlled by the oxide-carrier interaction, which influences both the structure and the dispersion of the active phase. In this case, the catalytic properties of MnO_x during ethanol oxidation depend on the type of support. Piumetti et al. [9] also investigated VOC oxidation on mesoporous manganese oxide catalysts and achieved the best results for Mn_3O_4 catalyst, which

* Corresponding author.
E-mail address: grazyna.straczewski@kit.edu (G. Straczewski).

https://doi.org/10.1016/j.jfueco.2021.100038
Received 20 May 2021; Received in revised form 6 September 2021; Accepted 17 October 2021
Available online 26 October 2021

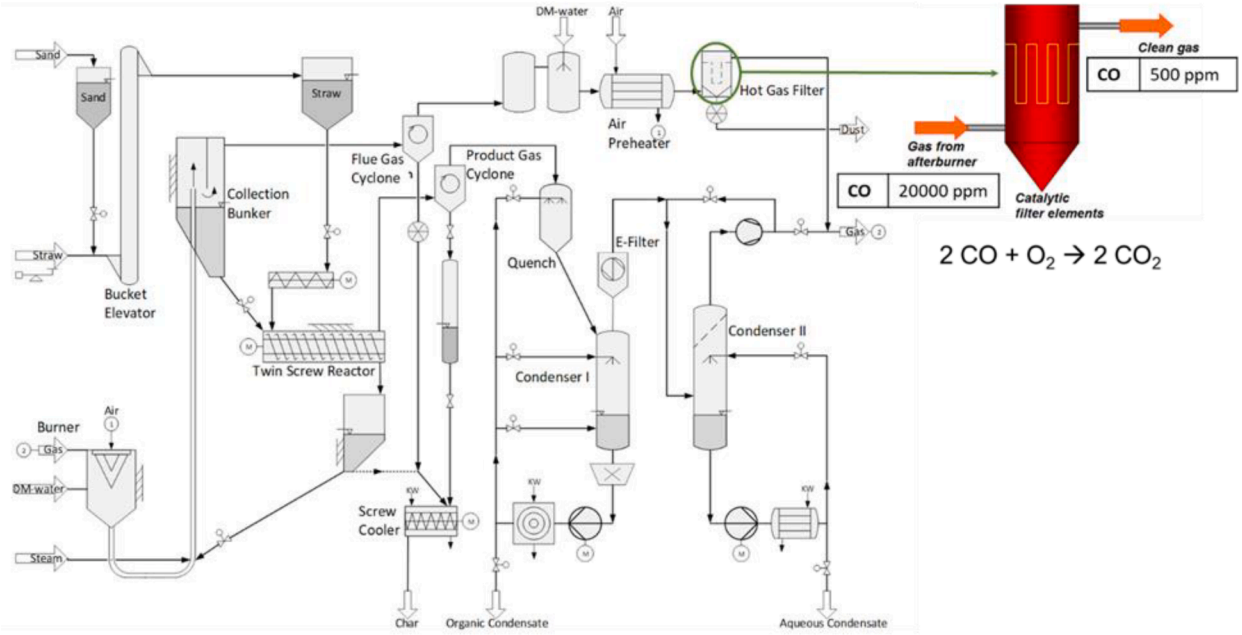

Fig. 1. Pyrolysis process in bioliq®.

showed the highest amount of electrophilic oxygens on the surface.

Oxidation of carbon monoxide at ambient temperature over amorphous mixed hopcalite-type catalysts has long been established and this type of catalyst is an accepted choice [14–19]. It is well known that at lower temperatures, copper-manganese oxides can catalyze the oxidation of CO and many compounds such as nitrogen-containing compounds, hydrocarbons, and other organic compounds that are often in the flue gasses [20,21]. The higher catalytic activity of binary oxide-supported Cu-Mn catalysts compared to pure oxide appears to be related to the existence of the mixed $Cu_{1.5}Mn_{1.5}O_4$ oxide. Many studies of the Cu-Mn catalyst system report the formation of mixed phases [22–25]. It has also been suggested that the charge transfer reaction $Cu^{2+} + Mn^{3+} \rightarrow Cu^{+} + Mn^{4+}$ ensures the high activity of the amorphous copper-manganese spinel (having the Mn:Cu ratio of 1:1) in the combustion reaction [20,21]. Buciuman et al. [15] proposed that the amorphous phase of Cu-Mn oxide is more active than the crystallized $CuMn_2O_4$ spinel because the catalytic activity of Cu-Mn oxides was influenced by the spillover model with manganese oxide as the oxygen donor and copper oxide as the oxygen acceptor.

The main idea of this study is to combine the advantage of the CuO_x–MnO_y catalyst system with a typical alumina-silicate fiber filter to obtain a new catalytic filter material in order to combine flue gas filtration with the conversion of undesired contaminants. To follow this idea the filter materials must be loaded with catalyst in such a way that on the one hand, they do not negatively affect the filter system and, on the other hand, the amount of catalyst must be sufficient for complete catalytic oxidation. Therefore, the "catalyst loading" in filter materials is an important parameter in a catalytic filter system. A set of catalytic CuO_x–MnO_y filter materials with different catalyst loadings was prepared by wet impregnation, characterized by XRD, BET, and SEM, and tested for the total oxidation of CO, VOC (ethene, ethane, propene, propane, 1-butene, n-butane, isobutane) and reduction of NO_2. Filter candles prepared from this catalytic material are aimed for oxidation of contaminants contained in the flue gas of a fast pyrolysis process to convert ash-rich biomass feedstocks into liquid bioliq [26] (see Fig. 1). By fast pyrolysis, the organic material is split into bio-oil as the main product, carbonized solid and non-condensable gas. In the pilot plant operated at KIT, for this process, biomass is mixed with hot sand in a twin-screw mixer reactor to provide rapid heating rates required for fast pyrolysis. After separation by gravity, the sand is circulated and heated up by hot combustion gasses in a so-called lift pipe at temperatures around 650 °C, allowing to form substantial amounts of CO of several hundred vppm. For practical reasons, the flue gas is combusted in the pilot plant after hot gas filtration together with the non-condensable pyrolysis gas. However, the pyrolysis gas can be used in commercial plants for energetic applications. In this case, post-combustion of the CO in the flue gas does not occur beneficially and will negatively influence the overall energy balance. Therefore, the combination of hot gas filtration with catalytic active materials appeared to be a promising technology, to which the first steps are described here.

Table 1
Catalyst loading of the filter material.

Filter	Cu [mg/cm^3]	Mn [mg/cm^3]
A0 – fixed bed	11.6	27.3
A0	11.6	27.3
A1	17.8	40.9
A2	23.7	54.5

Experimental

Catalyst preparation

All catalysts were prepared through wet impregnation method [4]. The copper nitrate ($Cu(NO_3)_2$•2.5 H_2O, Alfa Aesar, 98%) and manganese nitrate ($Mn(NO_3)_2$•4H_2O, Alfa Aesar, 98%) at the ratio of 1:2.3 (Cu:Mn) are dissolved in deionized water and stirred for 15 min. An aqueous solution of NaOH (1 N, Alfa Aesar) is added slowly to a mixed solution while stirring until the pH (pH Meter 691, Metrohm) of the solution reached a final pH of 10. Thereafter, the catalyst solution is stirred for one hour. Four catalytic solutions are prepared with the same Cu:Mn (1:2.3) stoichiometry, but different mass fractions (later called A0, A1, and A2 (see Table 1)). After preparation, the solution is sprayed several times in small portions onto the alumina-silicate (AlSi) filter plate of 130 mm x 160 mm in dimension (tested later as fixed bed) or onto 100 mm filter section with a diameter of 150 mm (tested later as catalytic filter). The support material is made of amorphous Al_2O_3(44%)/-SiO_2(56%) fiber composite with a porosity of 80 ~ 90% and a low pressure drop at high temperature of up to 1000 °C (Rath Group).

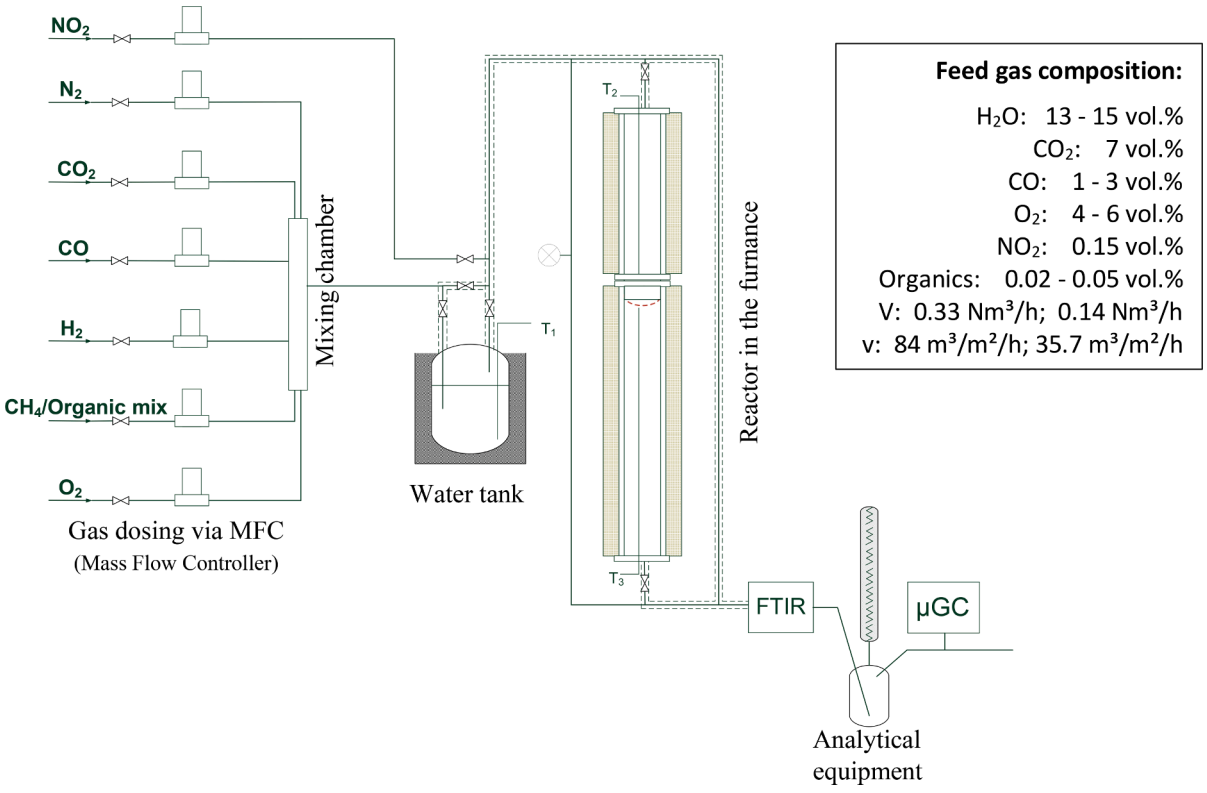

Fig. 2. Design of the lab-scale facility.

Between spraying, the filters materials are dried overnight at 80 °C. After spraying of all prepared solutions, the filter sections are dried again and finally calcined for 6 h at 450 °C in a ceramic furnace (Heraeus Instruments M110).

Catalyst characterization

The utilized catalytic materials were characterized before and after CO and VOC oxidation by BET (Brunauer-Emmett-Teller) physisorption. The texture characteristics were determined from the nitrogen adsorption isotherms obtained at −196 °C for samples degassed at 105 °C with a Quantachrome Nova 4000e specific surface area analyzer.

The catalyst samples are also investigated by X-ray diffraction using MPD Xpert-pro (PANalytical, Almelo, Netherlands) equipped with a multistrip PIXell detector (255 channels, 3.347°2Θ) and Cu radiation. Cu-Kβ was filtered with a Ni filter. The measurements were taken with soller slits of 0.04 rad (2.3°) and adjustable slits giving a constant irradiated sample length of 10 mm. For phase identification, the software packages Highscore-Plus (PANalytical) and Diffrac-Plus (Bruker-AXS, Karlsruhe, Germany) were used.

To investigate surface morphology and catalyst distribution in the support material, each of the catalysts is analyzed before and after the experiment by SEM (scanning electron microscope, Zeiss, Type Supra 55 VP) and EDXA (energy dispersive X-ray analysis, Bruker).

Catalyst testing

The catalytic tests are performed in a continuously operated stainless steel reactor of 10 cm diameter and 150 cm height at space velocities (GHSV) of 5000 and 8000 h^{-1}. In the first experiment (Chapter 3.2.1), the catalytic filter material as a fixed bed are mounted in a grid and installed in the downstream part of the tubular reactor. In the next experiments, the catalytic filter section is fixed in the flange and inserted into the tubular reactor with appropriate sealing materials (Isoplan 1000). Then, the two parts of the tubular reactor (see Fig. 2) are connected with screw bolts and hexagon nuts. The heating of the two-stage furnace is controlled by HORST controllers, by means of which the temperature program and the ramp rate can be set. The temperature is measured upstream and downstream of the catalytic filter bed or filter. The differential pressure of the tubular reactor was measured inductively with a pressure sensor (Digima ‑AP¨). The total gas feed of 0.33 m^3/h or 0.14 m^3/h (STP) with suitable gas composition (see Fig. 2) is passed through an electric preheater pipe before entering the reactor. The flow rates of synthetic air, CO_2, CO, and VOC or NO_2 are controlled using mass flow controllers (Bronkhorst High-Tech BV, Netherlands) and the LabVIEW system design software. The water is evaporated into a heated tank through which the stream of nitrogen is passed before reaching the preheater pipes. Temperatures of the water tank and heating pipes are adjusted and controlled with temperature controls (HORST). Downstream of the tubular reactor, analyzers are connected for online gas analysis. All pipe connections to the analytical equipment are heated to approximately 160 °C and controlled by a heating controller (WINKLER) to prevent the condensation of water. The concentrations of water vapor, CO_2, CO, NO_2, NO, and hydrocarbons in the gas downstream of the tubular reactor as well as downstream of the bypass were measured mainly by an FTIR (Fourier transform infrared spectrometer) analyzer (Gasmet Technologies) using the Calcmet software (Gasmet Technologies). In addition, concentrations of the gas components in the dry gas were monitored by µGC (micro Gas Chromatograph 490, Agilent Technologies).

Catalytic measurements are performed for estimating the light-off temperature of CO and VOC oxidation and NO_2 reduction in the temperature range of the set ramp-up period from 100 °C to a maximum of 600 °C. To determine long-term catalyst activity, data are collected continuously for about 100 h at a temperature of 390 °C.

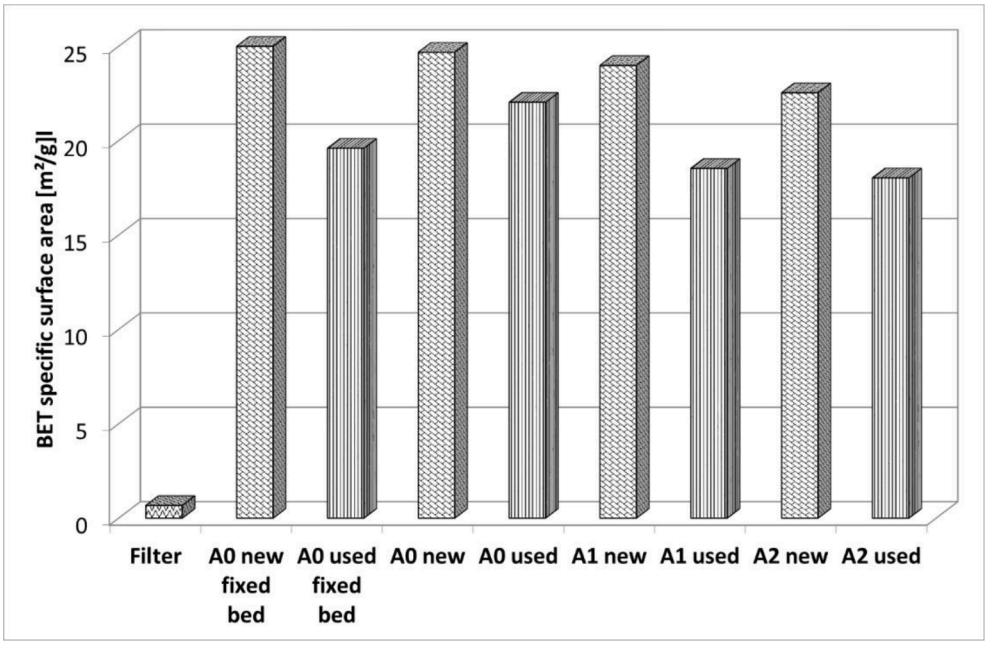

Fig. 3. BET surface areas of the pure filter material, fresh catalysts in the filter material, and used catalysts in the filter material.

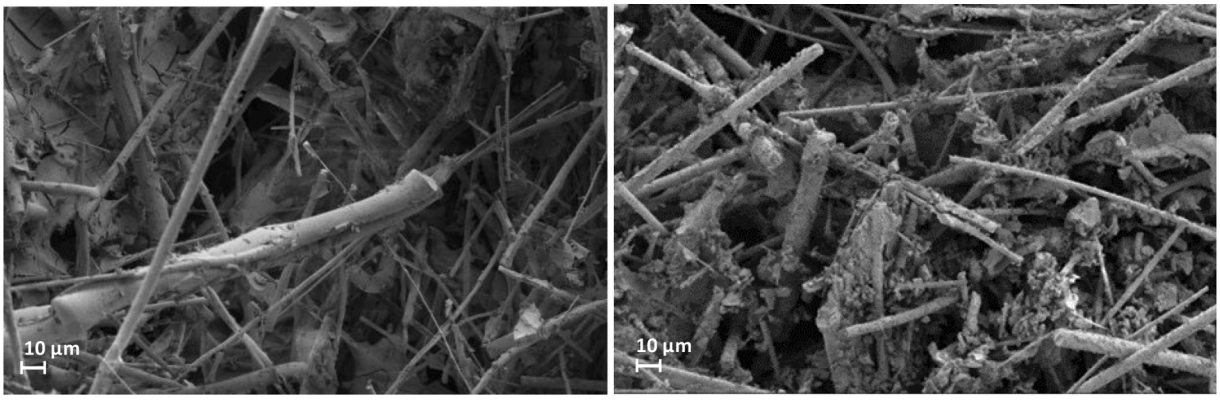

Fig. 4. SEM images of AlSi (left) and AlSi-CuO_x–MnO_y (right).

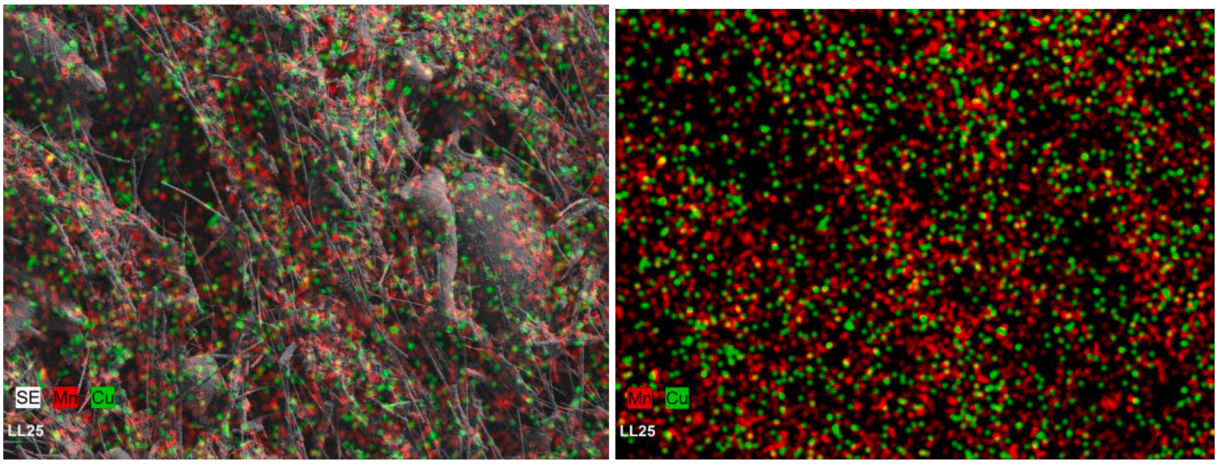

Fig. 5. EDXA images of Cu and Mn distribution in the AlSi support material.

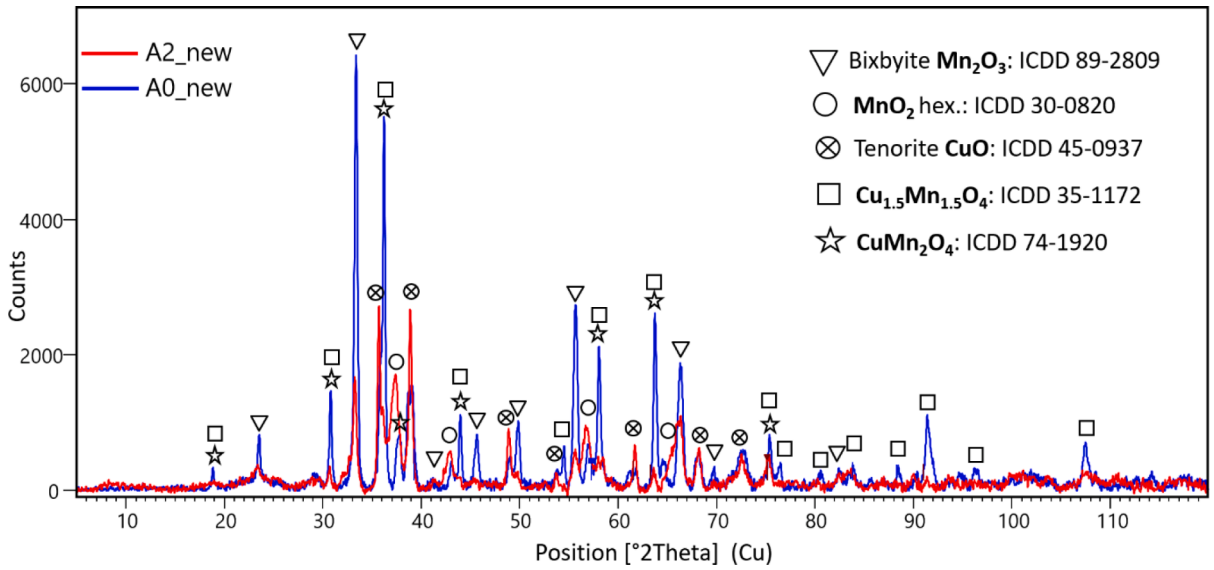

Fig. 6. X-ray diffraction of a new low-load (A0) and of a highly loaded Cu-Mn catalyst (A2) on amorphous aluminum silicate filter material.

Results and discussion

Catalyst morphology

BET surface area

According to Lowell et al. [27], BET surface area results reflect the adsorption capacities of the respective materials. The high surface area, i.e. the high adsorption capacity of the supported catalyst, determines the catalyst's high affinity for the combustion reaction.

The initial value of the surface area of alumina-silicate (AlSi) filter material is very low compared to that of the filter material with catalysts (see Fig. 3). The surface area of AlSi supported catalysts is about 35 times as large as that of the AlSi support material (0.65 m^2/g). AlSi support material has a very high porosity (80 to 90%) due to large spaces between the ceramic thread, but very low adsorption capacities due to the small amount of crystal structures. Small amounts of catalyst in the filter material result in a larger specific surface area, but in general, the differences between all three materials (A0, A1, and A2) are small. On the other hand, the surface areas of all catalysts used on the filter support decreased after CO/VOC oxidation. A specific surface area reduction of approximately 20% is found for the catalytic filters A1, A2, and fixed-bed catalytic filters A0. The surface area of A0 catalytic filters decreased by approximately 10% after CO/VOC oxidation. The decrease in specific surface areas might be caused by coke deposits that reduced the active surface area of the catalysts. Carbon deposition, coking, and moisture are the main causes of hopcalite catalyst deactivation [17]. On the other hand, this decrease of the BET specific surface area could be also explained by crystallization of the catalysts. Crystallization of amorphous catalysts is well known to cause sintering, thus leading to a decrease in the BET specific surface area [28].

SEM and EDX analysis

From SEM images of the support filter and catalyst on the filter elements, the catalyst location and distribution in the AlSi filter material were determined. Fig. 4 clearly shows the differences in distribution and adhesion of catalyst particles compared to the support filter material. Smaller and larger catalyst particles are distributed evenly along the alumina-silicate fibers. This catalyst distribution without cluster formation of the particles enables the best adsorption and later on the oxidation of the CO and VOC compounds. In addition, catalyst particles are attached so strongly to fiber material that they were not removed by typical filter operation without filter cleaning.

Elemental distribution of the Cu -Mn catalyst in the AlSi support materials is also estimated from EDXA analysis and is shown in Fig. 5. Each of the catalytic components is uniformly distributed inside the AlSi support material without any agglomerations.

XRD analysis

Not only is the distribution of the catalyst in the amorphous alumina-silicate important, but also the active catalyst structure plays a role. A small amount of copper prevents manganese oxide from assuming a highly ordered crystalline structure [29]. The disordered structure of manganese oxide results in the presence of oxygen vacancies, which leads to optimal combustion [20–21,24]. For this reason, the crystalline phases of new and used CuO_x–MnO_y catalysts were determined by X-ray diffraction for filters with low (A0), middle (A1), and high (A2) catalyst loading.

Fig. 6 shows a comparison of the XRD patterns of samples A2 new and A0 new. In addition to Mn_2O_3 (bixbyite), CuO (tenorite) the hexagonal polymorph of MnO_2, the new A0 filter material clearly shows a spinel structure with space group *Fd*-3 m and unit cell parameter of 8.295 Å. The XRD pattern lies in between two possible structures with compositions $Cu_{1.5}Mn_{1.5}O_4$ (8.274 Å) and $CuMn_2O_4$ (8.33 Å), respectively. Therefore, the spinel structure represents an isomorphic substitution between these two members. In contrast to this, the new A2 filter material contains much more hexagonal MnO_2 and CuO, also as a rare crystalline form of Cu_4O_3. Mn_2O_3 and spinel $CuMn_2O_4$ are in considerably lower quantity compared to A0 new sample (Fig. 6). The new filter material A1 reveals a completely different phase composition of the catalyst. While Mn_2O_3 and MnO_2 still predominate together with CuO, the spinel structures $CuMn_2O_4$ and Mn_3O_4 are in considerably lower amounts present. Many studies [22–25] published on the Cu-Mn catalyst system report the formation of a mixed spinel structure. The type of phase strongly depends on the synthesis conditions and results show a wide dispersion. At a calcination temperature above 550 °C, the mixed spinel structure is enriched in manganese and the composition tends to $CuMn_2O_4$ hopcalite [19,21]. In our case, the conditions of the catalyst synthesis and the calcination temperature were the same for all filter materials, only the amount of catalyst from one sample to another was always greater. The amount of co-deposited metal ions also appears to influence the formation of the $Cu_xMn_{3-x}O_4$ spinel and metal oxides. Hutchings et al. [18]. reported that phases of manganese copper mixed oxides in conjunction with CuO are less active than mixed oxide phases in conjunction with Mn_2O_3 in CO oxidation. In both the A0 and A2 catalytic filters, the Cu-Mn spinel occurs together with Mn_2O_3 and less with CuO. However, the presence of the spinel is more pronounced in

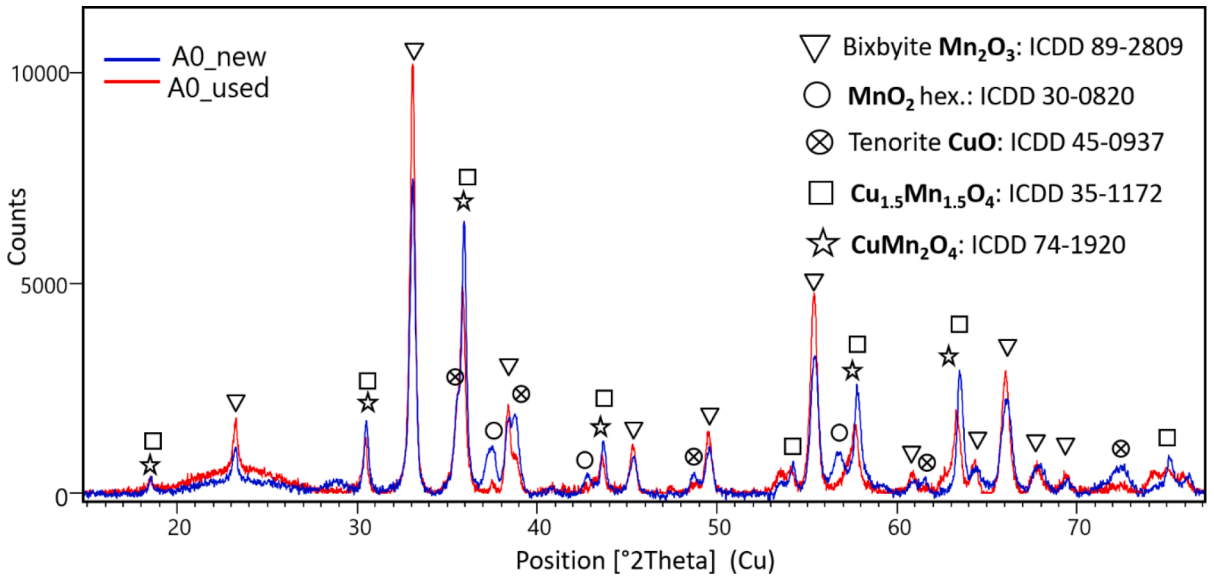

Fig. 7. X-ray diffraction of new and used A0 catalytic filters on amorphous aluminum silicate.

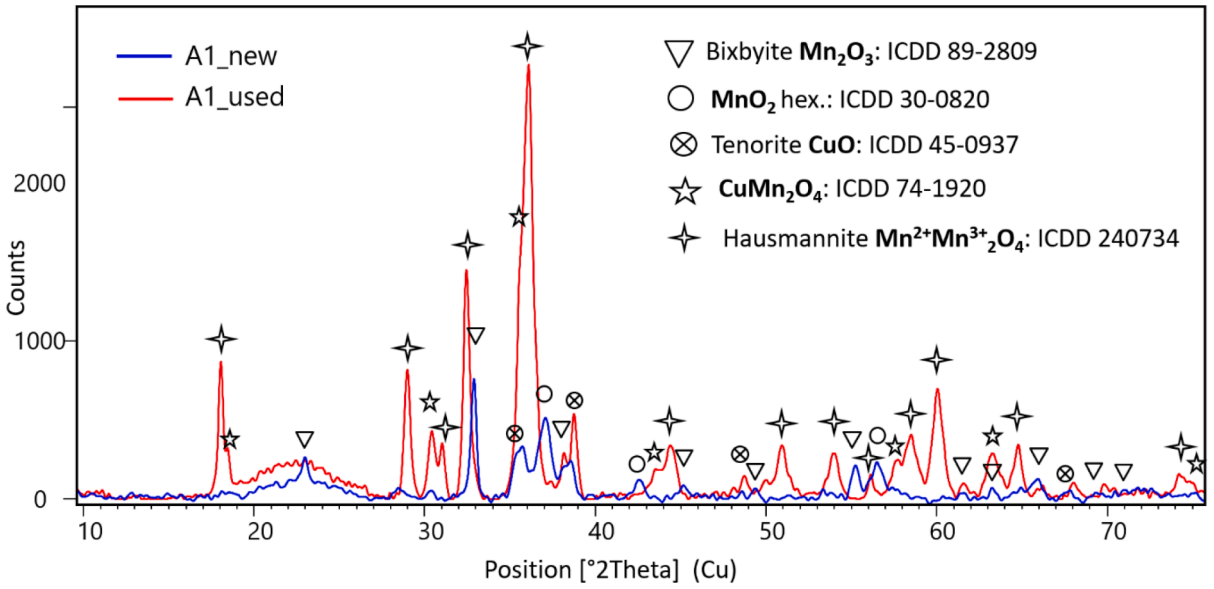

Fig. 8. X-ray diffraction of new and used A1 catalytic filters on amorphous aluminum silicate.

the A0 catalytic filter. Consequently, higher catalytic activities can be expected for this material. In the case of A1, the spinel phase is present in a lower quantity, as a result of which association with Mn_2O_3 is unlikely to enhance catalytic activities.

Fig. 7 shows a comparison between the XRD patterns of A0 new and A0 used samples. After using the catalytic A0 filter for oxidation, increased formation of Mn_2O_3 could be observed. The spinel phase, which can be represented by the general formula $Cu_xMn_{3-x}O_4$ is also clearly observed in the XRD pattern. A small shift of its peaks at lower 2Θ values (i.e. increase of the unit cell parameter) after oxidation could be interpreted as a change in the chemical composition toward Mn richer spinel. Further, significantly less CuO and hexagonal MnO_2 are observed. Similar changes in the phase composition of the catalyst are also found in the A2 catalytic filters used (Fig. 9). After oxidation, considerably more spinel is formed as a mixed structure of composition $Cu_xMn_{3-x}O_4$. In addition, the cubic bixbyite Mn_2O_3 (space group I a −3) is increasingly formed. In contrast, hexagonal MnO_2 and CuO (also Cu_4O_3) are not present. The phase composition of the catalyst in A1 differs considerably (see Fig. 8). Whereas the A1 new material consists predominately of bixbyite (Mn_2O_3), hexagonal MnO_2 and tenorite (CuO), the A1 used material shows the presence of mainly hausmannite, Mn_3O_4 and CuO. $CuMn_2O_4$ spinel is also formed, but in considerably smaller quantity compared to samples A0 and A2.

According to Figueroa et al. [7], catalytic activity is related to the presence of the Mn^{3+}-Mn^{4+} couple and Mn^{4+} vacancies, which results in the formation of OH groups, and a lower degree of crystallinity of the oxides. Exactly this couple Mn^{3+}-Mn^{4+} is found in the incomplete $Cu_{1.5}Mn_{1.5}O_4$ spinel existing in both catalytic filters used (A0, A2). Spassova et al. [24] also reported that interaction between Cu and MnO_x with the formation of a highly disordered mixed oxide of spinel-like structure is the cause of the high catalytic activity of the CuO-MnO_x catalyst. This interaction between Cu and MnO_x is present to a significantly lower extent in the new and used A1 filter material compared to A0 (see Fig. 10), since less $Cu_{1.5}Mn_{1.5}O_4$ spinel is formed. Therefore, this material can be expected to have low catalytic activity.

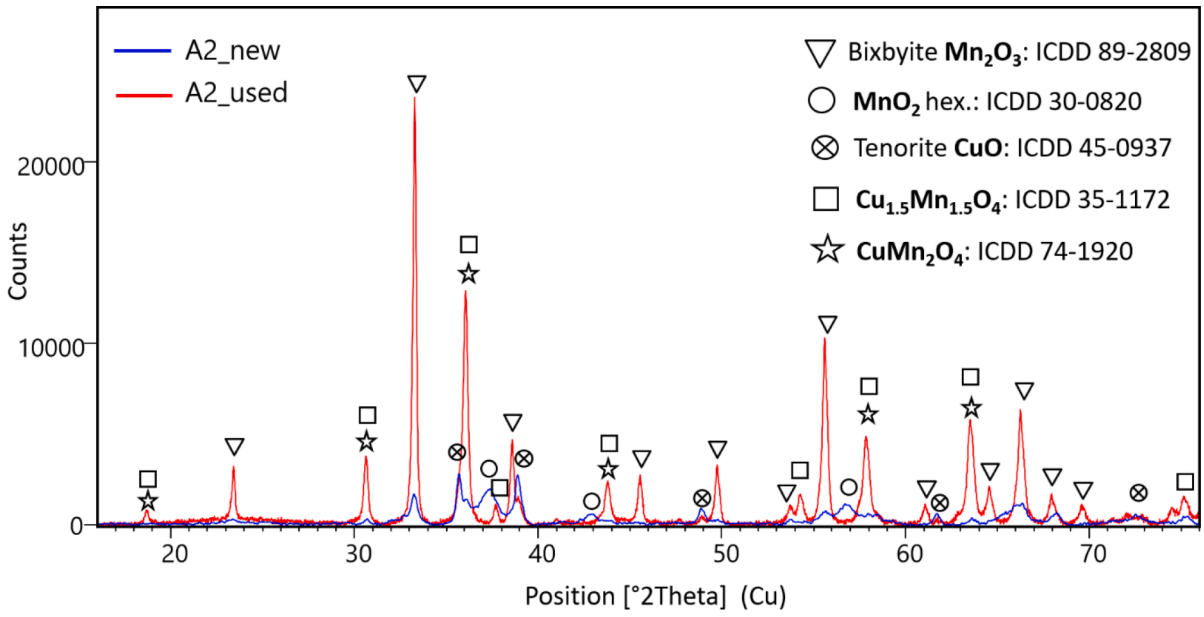

Fig. 9. X-ray diffraction of new and used A2 catalytic filters on amorphous aluminum silicate.

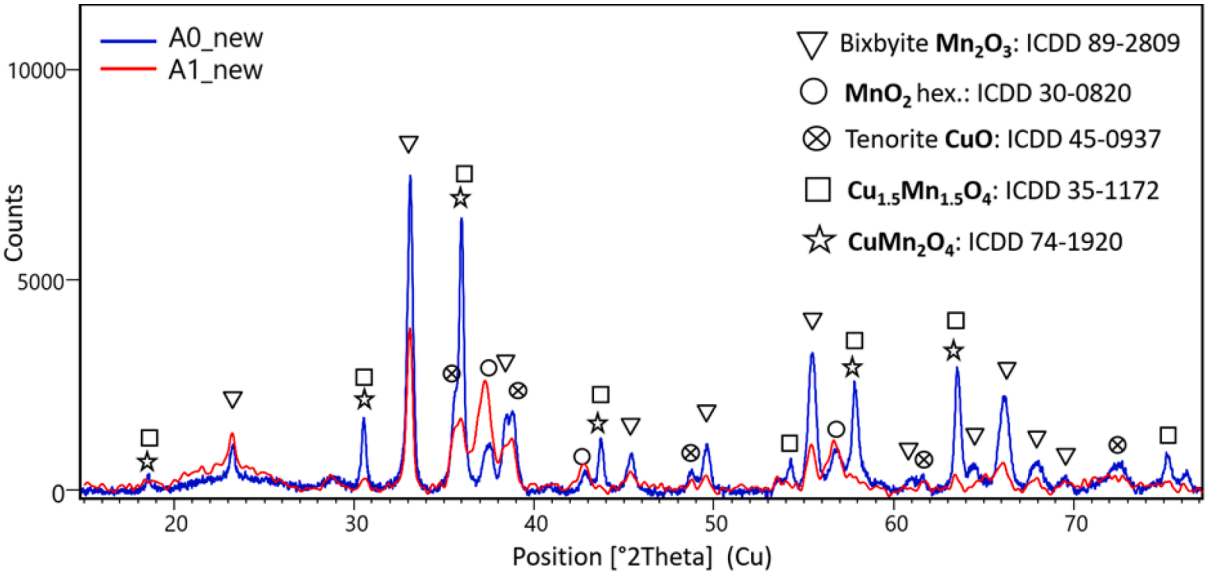

Fig. 10. X-ray diffraction of a new low-load (A0) and of a highly loaded Cu-Mn catalyst (A1) on the amorphous aluminum silicate filter material.

Catalyst activity

The catalytic activities in CO oxidation of the catalytic alumina-silicate fixed-bed filter (A0) and three samples of catalytic filters (A0, A1, and A2) were tested. The light-off temperatures of these catalytic materials were determined at a CO concentration of 1 to 3 vol.%, long-term stability was measured for a CO concentration of 2 vol.% only. The catalytic filter materials tested differed in the amounts of copper and manganese oxide, while the composition (stoichiometric Cu:Mn ratio) remained the same. For these experiments, the value of CO conversion was determined according to the following equation:

$$X_{CO}(\%) = \frac{C_{CO(in)} - C_{CO(out)}}{C_{CO(in)}} \cdot 100\% \quad (1)$$

where X_{CO}(%) is the carbon monoxide conversion,%; $C_{CO(in)}$ is the upstream CO concentration in the gas feed gas in vol.%; $C_{CO(out)}$ is the downstream CO concentration in vol.%.

In addition, catalytic activity in VOC oxidation of three catalytic filter samples (A0, A1, and A2) is measured. The light-off temperatures of these catalytic materials are determined for oxidation of ethane, ethane, propane, propene, 1-butene, butane, and isobutene. The value of every hydrocarbon conversion was determined according to the following equation:

$$X_{CH}(\%) = \frac{C_{CH(in)} - C_{CH(out)}}{C_{CH(in)}} \cdot 100\% \quad (2)$$

where X_{CH}(%) is the hydrocarbon conversion of every tested compound (ethane, ethane, propane, propene, 1-butene, butane, and isobutene),%; $C_{CH(in)}$ is the upstream hydrocarbon concentration, ppm; $C_{CH(out)}$ is the downstream hydrocarbon concentration, ppm.

The conversion of CO in reaction with NO_2 was also investigated for three catalytic filter samples (A0, A1, and A2). The light-off temperatures of these catalytic materials in this reaction ($2NO_2 + 4CO \rightarrow N_2 + 4CO_2$) are determined for CO concentrations of 1.5 vol.% and a constant

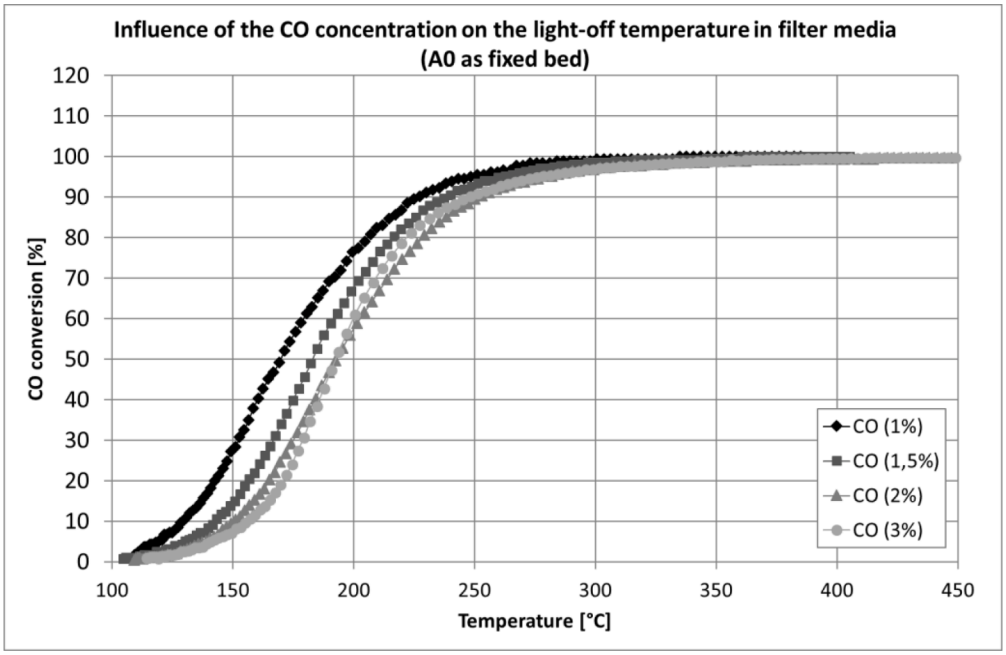

Fig. 11. Carbon monoxide conversion at CO concentrations from 1 to 3 vol.% over catalytic filter material (A0) in the form of a fixed bed, determination of light-off temperatures.

Table 2
The light-off temperature of the catalytic filter material.

Filter	CO [vol.%]	T_{50} [°C]	T_{90} [°C]
A0 – fixed bed	1	170	227
A0 – fixed bed	1.5	182	240
A0 – fixed bed	2	193	253
A0 – fixed bed	3	192	248

NO_2 concentration of 0.15 vol.%. The conversion of CO is calculated according to Eq. (1) and conversion of NO_2 according to the following equation:

$$X_{NO2}(\%) = \frac{C_{NO2(in)} - C_{NO2(out)}}{C_{NO2(in)}} \cdot 100\% \quad (3)$$

where X_{NO2}(%) is the nitrogen dioxide conversion,%; $C_{NO2(in)}$ is the upstream NO_2 concentration, ppm; $C_{NO2(out)}$ is the downstream NO_2 concentration, ppm.

CO oxidation over catalytic fixed-bed filter material

In order to find out whether catalyst loading with a small amount of catalyst in the filter material is sufficient for catalytic CO conversion, the catalytic filter material A0 is tested in the form of a fixed bed first. Fig. 11 shows the results for the combustion of carbon monoxide in the air. In this case, the low concentration of CO (1 vol.%) could be oxidized to CO_2 at a temperature which is about 30 °C lower. As the CO concentration increases, catalytic activity decreases, while the light-off temperature also increases (see Table 2). However, this catalytic filter material is comparatively active at higher CO concentrations (2 and 3 vol.%). Nevertheless, complete CO conversion [1] was achieved for all CO concentrations when the temperature exceeded 330 °C. Larson and Andersson [6] tested CuO_x, CuO_x-CeO_2, $CuMn_2O_4$, and Mn_2O_3 catalysts on Al_2O_3 supports. At a low CO concentration (0.2 vol%), a complete CO conversion of most of the tested catalyst combinations took place at about 200 °C. Only for CuO_x and Mn_2O_3 on the Al_2O_3 catalyst was 100% CO conversion achieved at around 250 °C already. Compared to our results for CuO_x–MnO_y catalysts on alumina-silicate filter material, the temperature needed for complete CO conversion was 100 °C higher, but CO concentration was five times higher. Taking into account that the light-off temperature of the complete CO conversion depends on the CO concentration and, hence, that a complete CO conversion of a lower CO concentration can be achieved at a lower temperature, our results fit quite well.

CO oxidation over a catalytic filter

Fig. 12 shows the results for the combustion of carbon monoxide in the air over the A0, A1, and A2 catalytic filters. Catalyst filter material A2 with a high load of CuO_x–MnO_y increases the activity for the combustion of CO. The addition of more catalysts substantially increases the activity for combustion of higher concentrations of CO (1.5–3 vol.%). If the filter material is highly loaded with CuO_x–MnO_y catalyst, the inlet temperature might be about 50 °C lower to achieve the same conversion rate compared to the A0 catalytic filter. The high loading of the filter material with catalyst significantly influences the activity. However, the filter material with low catalyst (A0) loading is better for combustion of small concentrations (up to 1.5 vol.%) of CO. In this case, the inlet temperature may be at least about 40 °C lower to obtain the same conversion rate as with A2. This is because the catalytic filter A0 reduces its catalytic activity with increasing carbon monoxide concentration and complete CO combustion takes place at ever-higher temperatures. With the A2 catalytic filter, on the other hand, catalytic activity increases with increasing carbon monoxide concentration and complete CO combustion takes place at ever-lower temperatures.

An increased amount of the CuO_x–MnO_y catalyst in the case of A1 decreases the activity for combustion of carbon monoxide, with the oxidation characteristic being completely different. With this loading of the filter material with CuO_x–MnO_y catalyst, the inlet temperature has to be around 100–200 °C higher to obtain the same CO conversion rate as with the A2 catalytic filter, for example XRD analysis (Chapter 3.1.3) reveals that the catalytic filter A1 mainly contains Mn_3O_4 and CuO catalytic material, which is less active than the spinel form of $Cu_xMn_{3-x}O_4$. Qian [30], Spassova [24], and Larsson [6] tested CuO_x, MnO_2, Mn_2O_3, and mixed CuO-MnO_x catalysts. They found that copper oxide and magnesium oxide, as well as the Cu-Mn mixed oxide without the spinel-like form $Cu_xMn_{3-x}O_4$ were much less active in CO conversion.

It can be concluded that alumina-silicate filter material highly loaded

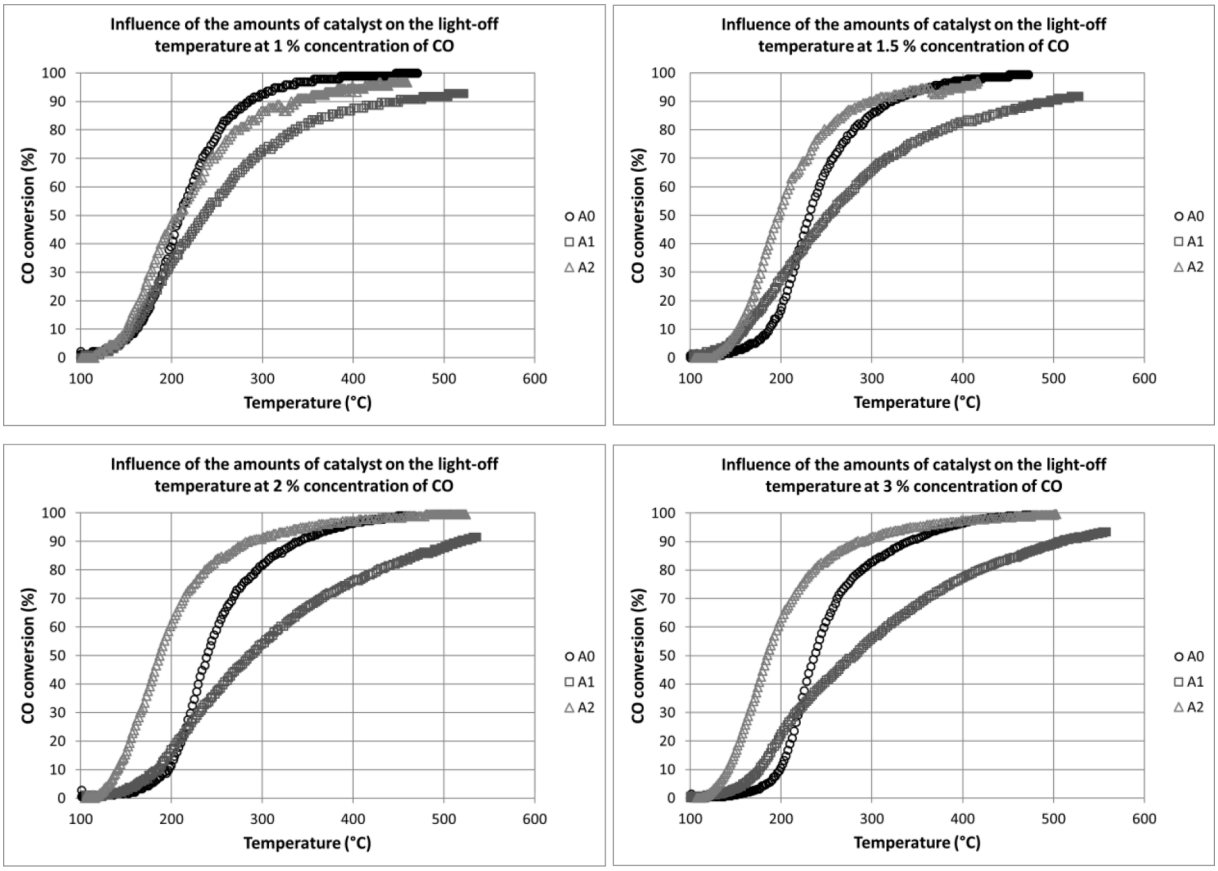

Fig. 12. CO conversion over the catalytic filter materials A0, A1, and A2, determination of light-off temperatures.

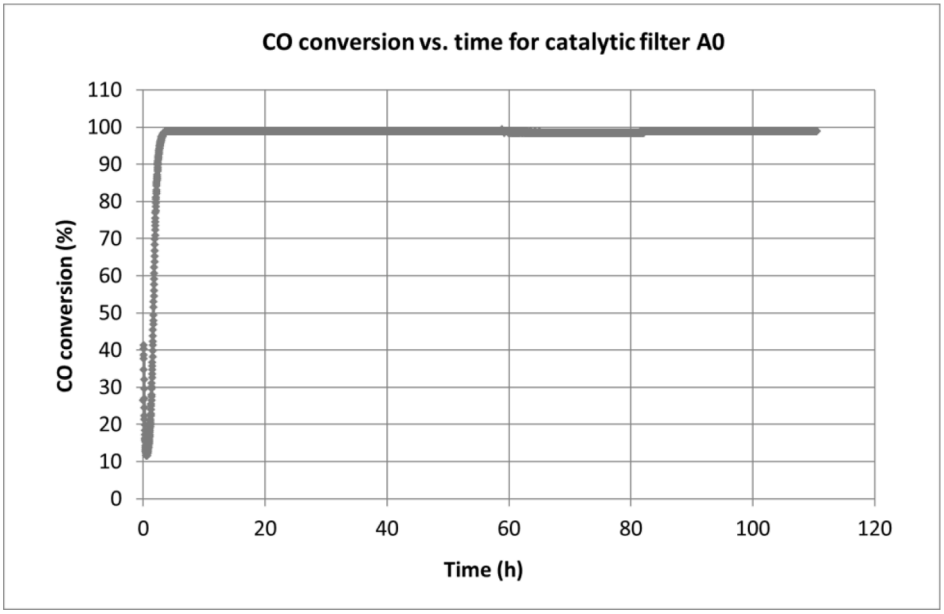

Fig. 13. CO conversions over catalytic filter material A0 as a function of time, temperature 390 °C.

with CuO_x–MnO_y catalyst enhances the total oxidation of highly concentrated CO.

When comparing the catalytic activities of an A0 fixed bed (Chapter 3.2.1) and an A0 filter, it is easy to see a shift to higher temperatures of the light-off temperatures T_{50} by about 40 °C and of T_{90} by about 80 °C. In both cases, the catalytic filter material certainly is equally active in CO oxidation, but the transport resistance of filters exceeds that of a fixed-bed filter. As a result, the catalytic activity can be shifted to higher temperatures.

Long-term stability tests are also carried out with respect to later practical use. CO (2 vol.%) oxidation is tested over all three filter materials A0, A1, and A2 at a temperature of 390 °C for more than 100 h.

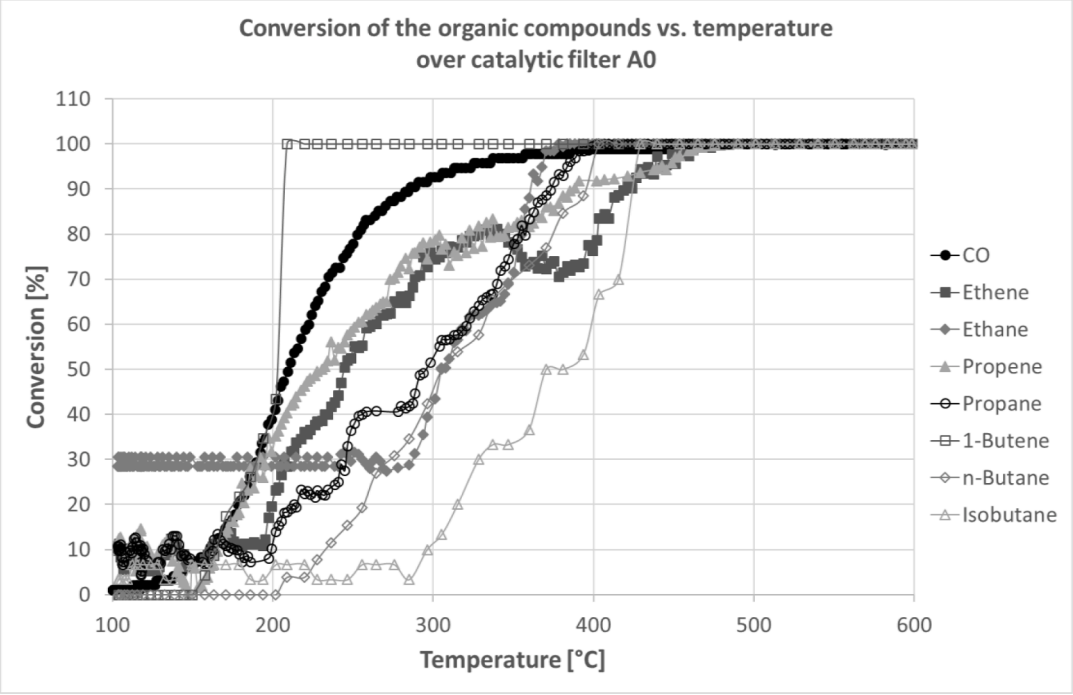

Fig. 14. Conversion of the mix of VOC (ethene, ethane, propene, propane, 1-butene, n-butane, isobutane) and CO over catalytic filter A0.

Table 3
Conversion of the mix of VOC and CO.

Component	A0 Temp. Conv.	A1 Temp. Conv.	A2 Temp. Conv.
1-butene	209 °C 100%	252 °C 100%	210 °C 100%
Isobutane	429 °C 100%	445 °C 100%	415 °C 100%
Ethene	475 °C 95%	490 °C 80%	470 °C 95%
Ethane	400 °C 100%	460 °C 100%	399 °C 100%
Propene	455 °C 100%	497 °C 80%	445 °C 100%
Propane	425 °C 100%	445 °C 100%	415 °C 100%
n-Butane	403 °C 100%	460 °C 100%	395 °C 100%
CO	280 °C 90%	500 °C 80%	275 °C 90%

Almost complete CO conversion [1] was measured for catalytic filter A0 (see Fig. 13) and A2. As expected, the CO conversion rate of catalytic filter A1 in this temperature range reached 75% only. However, no reduction in carbon monoxide conversion is observed for all three catalytic filter materials during the entire duration of CO combustion, which indicates a high activity of the catalyst.

VOC oxidation over the catalytic filter

Parallel oxidation of CO and VOC (gas mixture: Ethane, ethene, propene, propane, n-butane, 1-butene, isobutane) is studied for catalytic filter materials A0, A1, and A2. The following reactions of VOC were expected during the investigation:

$$2\ CH_3{-}CH_3 + 7\ O_2 \rightarrow 4\ CO_2 + 6\ H_2O \quad (4)$$

$$CH_2{=}CH_2 + 3\ O_2 \rightarrow 2\ CO_2 + 2\ H_2O \quad (5)$$

$$2\ CH_2{=}CH{-}CH_3 + 9\ O_2 \rightarrow 6\ CO_2 + 6\ H_2O \quad (6)$$

$$CH_3{-}CH_2{-}CH_3 + 5\ O_2 \rightarrow 3\ CO_2 + 4\ H_2O \quad (7)$$

$$2\ CH_3{-}CH_2{-}CH_2{-}CH_3 + 13\ O_2 \rightarrow 8\ CO_2 + 10\ H_2O \quad (8)$$

$$CH_2{=}CH{-}CH_2{-}CH_3 + 6\ O_2 \rightarrow 4\ CO_2 + 4\ H_2O \quad (9)$$

$$2\ CH_3{-}CHCH_3{-}CH_3 + 13\ O_2 \rightarrow 8\ CO_2 + 10\ H_2O \quad (10)$$

Almost complete conversion of organic substances was observed for the catalytic filters A0 (Fig. 14) and A2 up to 450 °C (see Table 3). The catalytic filter A2 with a high catalyst loading is found to be only slightly more active in organic and CO conversion. It is also important to note that during parallel oxidation of CO and VOC, the catalytic filters A0 and A2 are less active for the conversion of carbon monoxide. Probably due to the amount of CO_2 generated under these reaction conditions, carbon monoxide does not desorb quickly enough from the active center of the catalyst. Catalytic filter A1 is less active in the conversion of VOC and CO than the catalytic materials A0 and A2. At temperatures that are up to 50 °C higher than for the catalytic filters A0 or A2, an almost complete conversion [2] of organic substances is achieved (see Table 3). In the presence of organic compounds, CO conversion via this catalytic filter is slightly lower than without parallel oxidation of the VOC mixture. According to Tichenor and Palazzolo's report [31], alkanes und alcohols are the difficult extremes of oxidation. They studied non-halogenated VOC combustion over ceramic honeycombs coated with precious metal (platinum/palladium) and found that alcohols were most easily destroyed, followed by aldehydes, aromatics, ketones, acetates, and alkanes. They also found that the conversion rate of organic compounds depends not only on temperature, but also on space velocity, concentrations, and specific VOC incinerated in a mixture. Our investigation of VOC oxidation over a CuO_x–MnO_y catalytic filter revealed that the conversion rate depends not only on the class of organic compounds but also on the chain length. With respect to the conversion rate, the VOC mixtures can be ranked as follows: Long-chain alkenes > long-chain alkanes > alkanes > alkenes. Long-chain alkenes (1-butene) oxidize faster and alkenes (ethene, propene) more slowly.

CO—NO_2 reaction over the catalytic filter

Oxidation of CO by NO_2 in the CO—NO_2—O_2 and CO—NO_2 reactions is studied for catalytic filter materials A0, A1, and A2. The following competitive reactions may occur when the gas mixture is attached to the catalyst surface:

$$2\ NO_2 + 4\ CO \rightarrow N_2 + 4\ CO_2 \quad (11)$$

$$O_2 + 2\ CO \rightarrow 2\ CO_2 \quad (12)$$

$$NO_2 + CO \rightarrow CO_2 + NO \quad (13)$$

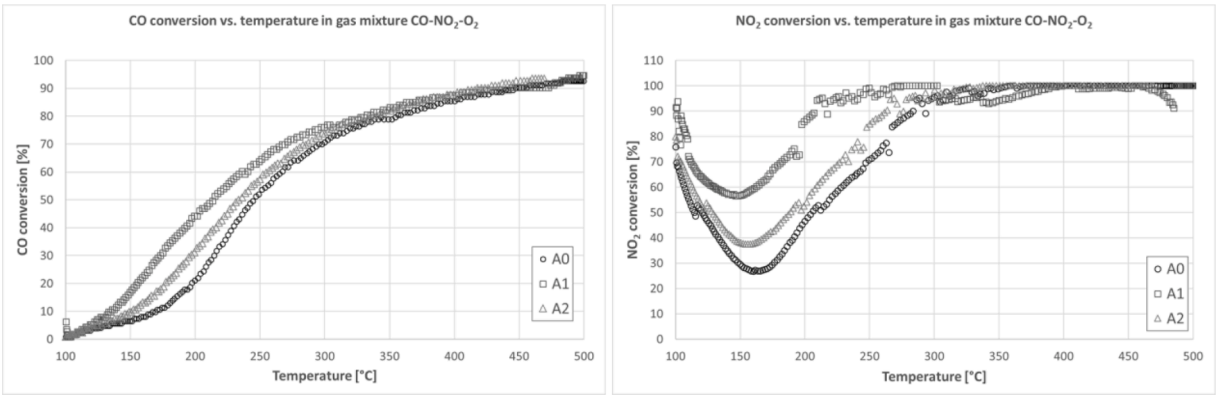

Fig. 15. CO conversion over catalytic filter materials A0, A1, and A2 (left) and nitrogen dioxide conversion over catalytic filter materials A0, A1, and A2 (right) in the gas mixture CO—NO_2—O_2.

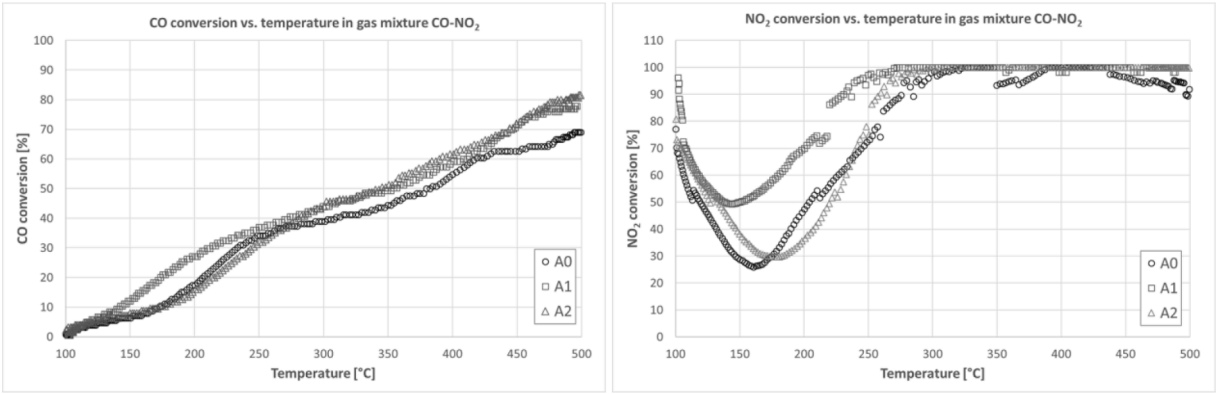

Fig. 16. Carbon monoxide conversion over catalytic filter materials A0, A1, and A2 (left) and nitrogen dioxide conversion over catalytic filter materials A0, A1, and A2 (right) in the CO—NO_2gas mixture.

$$2\ NO + 2\ CO \rightarrow N_2 + 2\ CO_2 \quad (14)$$

An analysis of the behavior of the CO—NO_2—O_2 gas mixture over the catalytic filters indicated that reactions [12] and [13] predominate. However, a comparison of CO conversion [1] with and without NO_2 (Chapter 3.2.2) showed that filters A0 and A2 are less active due to NO_2 (see Fig. 15). The additional adsorption of NO_2 or NO (from reaction [13]) on the catalyst surface inhibited the rapid reaction between CO and O_2 in the higher temperature range. Kapteijn et al. [32] found that NO interacts very weakly with the manganese oxide surface on alumina (2–8.4 wt% Mn). Strongly oxidized species are formed in the presence of oxygen, resulting in nitrite and nitrate groups. These species decompose, thus releasing NO gas which is largely adsorbed on the catalyst surface.

For the catalytic filter A1, however, much stronger activity in the CO oxidation [1] is observed, which is even more pronounced in the presence of NO_2. This increase in catalytic activity may only reflect a parallel reaction [13] and a lower adsorption affinity for NO of this catalyst composition. Although Spassova et al. [24]. suggest that oxygen initially has some positive effect on the CO—NO reaction, gradual deactivation of the surface of CuO-MnO_x samples with time was observed. It may be caused by the slow regeneration of active sites. The rate may be limited by the slow desorption of the reaction product CO_2. Due to the adsorption of NO_2/NO, it is strongly bound to the catalyst's active sites.

The reduction of NO_2 with a conversion rate of 100% [3] took place at a relatively low temperature (below 300 °C), but an increase in the NO concentration was observed. This atypical NO_2 conversion curve could be related to the partial inhibition of the NO_2 gas-phase reaction with increasing temperature. During this phase, the concentration of nitrogen monoxides increases. Although simultaneous adsorption of CO and NO_2 could occur, it is assumed that during the initial transition period, CO first interacts with the oxygen from the catalyst surfaces. At the same time, the degree of CO conversion into CO_2 is quite good, while NO_2 conversion into N_2 does not take place. Spassova et al. [24]. also suggest that the formation of NO_2 and its subsequent interaction with CO might be key steps for the mechanism of NO reduction to N_2 on the surface of CuO-MnO_x catalysts under the oxidizing conditions. With increasing temperature (from 25 °C to 50 °C), adsorbed NO_2 decomposes with elution of NO or reacts with CO to release NO. The reaction CO—NO_2 was observed to predominate in the production of CO_2 and NO. NO was found to react with O_2 to other more reactive species, which in the next step, together with CO are reduced directly to N_2.

Investigation of the behavior of the gas mixture CO—NO_2 as a function of the catalytic filters revealed that reactions [13,14] are gradual. At higher temperatures (above 350 °C), reaction [11] may also take place. CO conversion [1] overall three catalytic filter materials A0, A1, and A2 are much lower in the absence of oxygen (see Fig. 16). NO_2, however, is converted much faster with a significant decrease in NO concentration. At the lower temperature (100 – 350 °C), CO reacts with only one oxygen from NO_2 and the products are CO_2 and NO. At higher temperatures (above 350 °C), NO also reacts with CO and conversion of CO into CO_2 and of NO_2 into N_2 was observed. It is logical to assume that the degrees of NO_2 conversion achieved could be related to the amount of NO desorbed after this stage. It is the competition between catalyst surface oxygen and NO for interaction with CO that defines the rate of N_2 production. Spassova et al. [24] also found that high degrees of NO into N_2 conversion (up to 100%) when increasing the temperature up to 300 °C. In this temperature region, measurable steady-state conversions

Table 4
Conversion of the mix of VOCs and CO after tests with NO_2.

Component	A0 Temp. Conv.	A1 Temp. Conv.	A2 Temp. Conv.
1-butene	330 °C 100%	323 °C 100%	312 °C 100%
Isobutane	500 °C 65%	484 °C 100%	500 °C 70%
Ethene	454 °C 50%	500 °C 30%	470 °C 55%
Ethane	500 °C 45%	430 °C 52%	500 °C 55%
Propene	465 °C 80%	500 °C 68%	485 °C 75%
Propane	485 °C 70%	500 °C 80%	500 °C 75%
n-Butane	490 °C 75%	500 °C 97%	495 °C 77%
CO	500 °C 80%	500 °C 75,5%	500 °C 80%

of NO into N_2 are attained in CO+NO+Ar, i.e. the reduction of NO to N_2 is fast enough to compete with the CO—O_{surf} reaction. Gassan-zadeh et al. [33]. studied the catalytic reduction of nitrogen oxides by carbon monoxide over NiO and found that it is fast enough to compete with the CO—O_2 reaction. For the CO—NO—O_2 interaction, an interaction between CO- and NO_2-related intermediates is suggested to eventually generate N_2 and CO_2.

VOC oxidation after NO_2 reduction over the catalytic filter

In the next step, parallel oxidation of carbon monoxide and VOC over the catalytic filter materials A0, A1, and A2 is studied after testing the catalytic filters in the CO—NO_2 reaction. The influence of the reaction on the catalyst activity was investigated. In this case, all three catalytic filters are less active in organic oxidation (see Table 4 and Fig. 17). Complete conversion [2] on all three catalytic filters is only achieved for 1-butene at a temperature below 330 °C. Conversion of the remaining organic substances is not complete even at 500 °C and differed for each component. The catalytic filter with a high catalyst load (A2) converted organic compounds into CO_2 at a rate of 55–80%. The second catalytic filter A0 is only slightly less active than A2 and converted residual organic compounds at a rate of 45–80%. Catalytic filter A1, which previously had not been as active as A0 and A2, appeared to be somewhat more active after the CO—NO_2 reaction. Probably due to the formation of new, more active crystal structures from Mn_2O_3, MnO_2, and CuO. This catalytic filter is found to convert almost 100% isobutane and n-butane at temperatures below 500 °C, whereas the conversion rate of the remaining organic compounds was 30–80% only. All three catalytic filters are also less active for the conversion of carbon monoxide in the parallel oxidation of CO and VOC. Compared to the data measured before, the catalytic filters A0 and A2 are less active, while catalytic filter A1 hardly changed its CO conversion [1] activity. Obviously, the CO—NO_2 reaction has a bigger impact on catalysts on alumina-silicate filter material. Changes in the crystal structure of the catalyst are supposed to make the catalysts less active for CO and VOC oxidation. In part, the lower activity of the catalyst could be explained by the slower desorption of CO_2 from the active center of the catalyst, but this certainly is not the only effect.

The ranking proposed above for VOC oxidation on CuO_x–MnO_y catalytic filters of long-chain alkenes > long-chain alkanes > alkanes > alkenes has changed after testing the catalytic material in the CO—NO_2 reaction. A general ranking cannot be established for all three catalytic filter materials, although catalytic filter A1 largely follows the classification suggested and filters A0 and A2 have very similar activity. The following rankings currently apply to the catalytic filter:

A0 1-butene > propene > *n*-butane > propane > isobutane > ethene > ethane,
A1 1-butene > isobutane > *n*-butane > propane > propene > ethane > ethene,
A2 1-butene > *n*-butane > propane=propene > isobutane > ethene=ethane.

Conclusion

A series of catalytic alumina-silicate (fiber material) filters with different loadings of CuO_x–MnO_y catalyst is produced and investigated in the oxidation of CO, VOC, and CO in the presence of NO_2. The manufactured catalytic filters are characterized by a uniform distribution of catalyst material along with the fiber material of the support. By means of XRD of filters A0 and A2 with the CuO_x–MnO_y catalyst, incomplete spinel structures in the forms $Cu_{1.5}Mn_{1.5}O_4$ and $CuMn_2O_4$ are identified. Complete CO oxidation on catalytic filters (A0 fixed bed and A0 and A2 filters) with 100% conversion is reached in the temperature range from 200 to 500 °C. The catalysts on the filter material

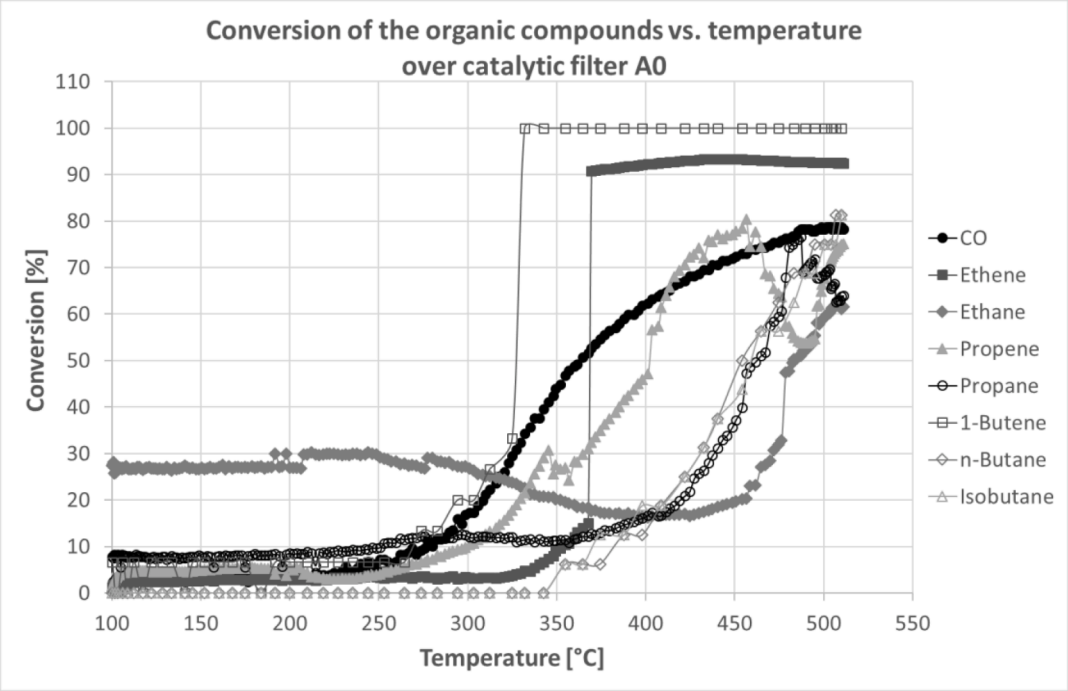

Fig. 17. Conversion of the mix of VOC (ethene, ethane, propene, propane, 1-butene, n-butane, isobutane) and CO on catalytic filter A0 after tests with NO_2.

Table A.1
: The light-off temperatures of the different catalytic filters.

Filter	CO [vol.%]	T_{50} [°C]	T_{90} [°C]
A0	1	204.3	288.5
A0	1.5	224	310
A0	2	238	336
A0	3	234	337.5
A1	1	225.5	425.5
A1	1.5	260	504
A1	2	281.4	522
A1	3	281.5	512.5
A2	1	191	334.8
A2	1.5	203.8	311.8
A2	2	190	288.5
A2	3	185.5	282

were not deactivated during tests for more than 100 operating hours. After this time, no visible changes were observed in the catalytic filter. XRD characterization of the catalytic filters reveals that the spinel structure formation of the catalyst is more pronounced (A0, A2). For CO oxidation in the presence of NO_2 on CuO_x–MnO_y catalytic filters, the catalytic activity was found to decrease significantly on filters A0 and A2 and to increase on filter A1. Filter A1 is even more active than in the previous tests. At the same time, reduction of NO_2 by CO below 300 °C is completed, but with increasing NO concentration. For CO oxidation with NO_2 on CuO_x–MnO_y catalytic filters, a further decrease in the catalytic activity is observed on all catalytic filters. However, NO_2 is reduced even faster, with the NO concentration decreasing significantly. Complete VOC oxidation on the catalytic filters (A0, A2) is achieved in the temperature range from 200 to 475 °C. The catalytic filter A1 is less active for VOC oxidation due to the low quantity of an incomplete spinel structure in the catalyst. Depending on the conversion rates of the tested organic compounds, the following oxidation ranking is proposed: Long-chain alkenes > long-chain alkanes > alkanes > alkenes. After CO—NO_2 interaction, the catalytic activity of VOC oxidation on the catalytic filters is found to decrease to about 50% to 80%. The respective application of the wet impregnation of CuO_x–MnO_y catalyst to full-size AlSi ceramic filter and testing of these catalytic candles in the flue gas of a fast pyrolysis process have to be further investigated at KIT.

Funding

This research did not receive any specific grant from funding agencies in the public, commercial, or not-for-profit section.

Declaration of Competing Interest

The authors declare that they have no known competing financial interests or personal relationships that could have appeared to influence the work reported in this paper.

Acknowledgments

The authors would like to especially thank Mr. Herbert Fischer for SEM/EDXA investigations as well as Dr. Günter Beuchle for the BET measurements. We acknowledge support from the KIT-Publication Found at the Karlsruhe Institute of Technology.

Appendix

Table A.1

References

[1] Speight JG. Chapter 2: 2.4 complete and incomplete combustion. Handbook of industrial hydrocarbon process. 2nd ed. United Kingdom: Gulf Professional Publishing; 2020. p. 45–93 (ISBN 978-0-12-809923-0).
[2] Granger P. Challenges and breakthroughs in post-combustion catalysis: how to match future stringent regulations. Catal Sci Technol 2017;7:5195–211.
[3] Wang CH, Lin SS, Chen CL, Weng HS. Performance of the supported copper oxide catalysts for the catalytic incineration of aromatic hydrocarbons. Chemosphere 2006;64:503–9.
[4] Delimaris D, Ioannides T. VOC oxidation over CuO-CeO_2 catalyst prepared by a combustion method. Appl Catal B 2009;89:295–302.
[5] Larsson PO, Andersson A, Wallenberg LR, Svensson B. Combustion of CO and toluene; characterisation of copper oxide supported on titania and activity comparisons with supported cobalt, iron and manganese oxide. J Catal 1996;163:279–93.
[6] Larsson PO, Andersson A. Oxides of copper, ceria promoted copper, manganese and copper manganese on Al_2O_3 for the combustion of CO, ethyl acetate and ethanol. Appl Catal B 2000;24:175–92.
[7] Figueroa SJA, Requejo FG, Lede EJ, Lamaita L, Peluso MA, Sambeth JE. XANES study of electronic and structural nature of Mn-sites in manganese oxides with catalytic properties. Catal Today 2005;107-108:849–55.
[8] Trawczyński J, Bielak B, Miśta W. Oxidation of ethanol over supported manganese catalysts – effect of the carrier. Appl Catal B 2005;55:277–85.
[9] Piumetti M, Fino D, Russo N. Mesoporous manganese oxides prepared by solution combustion synthesis as catalysts for the total oxidation of VOCs. Appl Catal B 2015;163:277–87.
[10] Hettige C, Mahanama KRR, Dissanayake DP. Cyclohexane oxidation and carbon deposition over metal oxide catalysts. Chemosphere 2001;43:1079–83.
[11] Saqer SM, Kondarides DI, Verykios XE. Catalytic activity of supported platinum and metal oxide catalysts for toluene oxidation. Top Catal 2009;52:517–27.
[12] Delimaris D, Ioannides T. VOC oxidation over MnOx–CeO_2 catalysts prepared by a combustion method. Appl Catal B 2008;84:303–12.
[13] Li S, Wang H, Li W, Wu X, Tang W, Chen Y. Effect of Cu substitution on promoted benzene oxidation over porous CuCo-based catalysts derived from layered double hydroxide with resistance of water vapor. Appl Catal B 2015;166-167:260–9.
[14] Musick JK, Williams FW. Catalytic decomposition of halogenated hydrocarbons over hopcalite catalyst. Ind Eng Chem Prod Res Dev 1974;13:175–9.
[15] Buciuman FC, Patcas F, Hahn T. A spillover approach to oxidation catalysis over copper and manganese mixed oxides. Chem Eng Process 1999;38:563–9.
[16] Chen H, Tong X, Li Y. Mesoporous Cu-Mn hopcalite catalyst and its performance in low temperature ethylene combustion in a carbon dioxide stream. Appl Catal A 2009;370:59–65.
[17] Dey S, Dhal GC. Deactivation and regeneration of hopcalite catalyst for carbon monoxide oxidation: a review. Mater Today Chem 2019;14:100180.
[18] Hutchings GJ, Mirzaei AA, Joyner RW, Siddiqui MRH, Taylor SH. Ambient temperature CO oxidation using copper manganese oxide catalyst prepared by coprecipitation: effect of ageing on catalyst performance. Catal Lett 1996;42:21–4.
[19] Hutchings GJ, Mirzaei AA, Joyner RW, Siddiqui MRH, Taylor SH. Effect of preparation conditions on the catalytic performance of copper manganese oxide catalysts for CO oxidation. Appl Catal A Gen 1998;166:143–52.
[20] Puckhaber LS, Cheung H, Cocke DL, Clearfield A. Reactivity of copper manganese oxides. Solid State Ionics 1989;32-33:206–13.
[21] Vepřek S, Cocke DL, Kehl S, Oswald HR. Mechanism of the deactivation of hopcalite catalysts studied by XPS, ISS, and other techniques. J Catal 1986;100:250–63.
[22] PalDey S, Gedevanishavili S, Zhang W, Rasouli F. Evaluation of a spinel based pigment system as a CO oxidation catalyst. Appl Catal B 2005;56:241–50.
[23] Tanaka Y, Takeguchi T, Kikuchi R, Eguchi K. Influence of preparation method and additive for Cu-Mn spinel oxide catalyst on water gas shift reaction of reformed fuels. Appl Catal A 2005;279:59–66.
[24] Spassowa I, Khristova M, Panayotov D, Mehandjiev D. Coprecipitated CuO-MnOx catalyst for low-temperature CO-NO and CO-NO-O_2 reactions. J Catal 1999;185:43–57.
[25] Papavasiliou J, Avgouropoulos G, Ioannides T. Steam reforming of methanol over copper–manganese spinel oxide catalysts. Catal Commun 2005;6:497–501.
[26] Pfitzer C, Dahmen N, Tröger N, Weirich F, Sauer J, Günther A, Müller-Hagedorn M. Fast pyrolysis of wheat straw in the bioliq pilot plant. Energy Fuels 2016;30:8047–54.
[27] Lowell S, Shields JE, Thomas MA, Thommes M. Characterisation of porous solids and powders: surface are, pore size and density. Netherlands: Kluwer Academic Publishers; 2004.
[28] Li WB, Zhuang M, Wang JX. Catalytic combustion of toluene on Cu-Mn/MCM-41 catalysts: influence of calcination temperature and operating conditions on the catalytic activity. Catal Today 2008;137:340–4.
[29] Morales MR, Barbero BP, Cadus LE. Evaluation and characterisation of Mn-Cu mixed oxide catalysts for ethanol total oxidation: influence of copper content. Fuel 2008;87:1177–86.
[30] Qian K, Qian Z, Hua Q, Jiang Z, Huang W. Structure-activity relationship of Cu/MnO_2 catalysts in CO oxidation. Appl Surf Sci 2013;273:357–63.
[31] Tichenor BA, Palazzolo MA. Destruction of volatile organic compounds via catalytic incineration. Environ Prog 1987;6:172–6.
[32] Kapteijn F, Singoredjo L, Vandriel M, Andreini A, Moulijn JA, Ramis G, Busca G. Alumina-Supported manganese oxide catalysts: II. Surface characterization and adsorption of ammonia and nitric oxide. J Catal 1994;150:105–16.
[33] Gassan-zade GZ, Mukherjee TK, Alkhazov TG. Effect of oxygen on the catalytic reduction of nitric oxides by carbon monoxide over NiO. Reaction Kinetics and Catalysis Letter 1979;12:525–9.